

BaCaF₂/III–V semiconductor broadband distributed Bragg reflectors for long-wavelength VCSEL and SESAM devices

Anna Koeninger · Gerhard Boehm ·
Ralf Meyer · Markus-Christian Amann

Received: 13 June 2014 / Accepted: 15 September 2014 / Published online: 27 September 2014
© Springer-Verlag Berlin Heidelberg 2014

Abstract Semiconductor devices such as vertical-cavity surface-emitting lasers (VCSELs) or semiconductor-saturable absorber mirrors (SESAMs) require high-reflection mirrors. Moreover, in VCSELs, it is beneficial to have a crystalline mirror, which is as thin as possible in order to ensure a high thermal conductivity for efficient heat-sinking of the laser. On the other hand, the wavelength tuning range of a SESAM is limited by the reflection bandwidth of its distributed Bragg reflector (DBR). Thus, broadband mirrors are preferable here. This paper reports a three-pair DBR grown by molecular beam epitaxy (MBE) using BaCaF₂ and GaAs on a GaAs (100) substrate. Due to the high ratio in refractive indices of GaAs and the group-IIa-fluorides, high-reflectivity mirrors and wide bandwidths can be obtained with low total thicknesses. We also investigated growth and stability of the material BaCaF₂, as well as its thermal conductivity both as single layer and Bragg reflector. Observed peeling of the layers could be avoided by implementing a fluorine treatment previous to the BaCaF₂ growth.

1 Introduction

Distributed Bragg reflectors with broad reflection bandwidths and good thermal properties are desirable for many applications. For example, tunable VCSELs with a state-of-the-art semiconductor DBR are all limited in their tuning range by a narrow stopband. Indeed, using

combinations with dielectrics leads to a broadening of the reflection bandwidth and a decrease in total mirror thickness necessary to achieve the same high reflectivity. But often these materials can only be evaporated amorphously or polycrystalline, which decreases thermal conductivity. Therefore, materials are needed that have a great difference in refractive indices and can be grown in a crystalline or polycrystalline structure. A promising material combination to fulfill all these requirements consists of III–V semiconductors and group-IIa-fluorides. For example, in the year 2000, the successful usage of CaF₂ in GaAs-based SESAMs was reported [1].

From Fig. 1, it can be seen that the lattice constants of group-IIa-fluorides BaF₂ and CaF₂ envelop with 0.62 and 0.55 nm, respectively, most III–V semiconductor materials. Because the fluorite lattice (left inset in Fig. 1) is closely related to the zinkblende lattice (right inset) [2], epitaxial growth can be expected. Therefore, it is possible to use lattice-matched BaCaF₂ to substitute the low-index material of a III–V-DBR. For example, in InP-based VCSELs, this would mean to replace AlInAs by BaCaF₂. On the one hand, a dielectric crystalline mirror will enhance heat dissipation through the device. On the other hand, it will permit a very short-cavity device, which enables high-frequency operation, too. The interested reader can find detailed information about short-cavity VCSEL design in Ref. [3]. By adjusting the BaF₂ content, BaCaF₂ can also be grown lattice matched on GaAs, e.g., for SESAMs (AlAs would be substituted here).

In this work, we used a material combination of GaAs and BaCaF₂ to implement a DBR with high contrast in refractive index ($\Delta n \approx 2$) that can be grown by MBE. Hence, high reflectivities can be accomplished by a small number of pairs. Similar approaches can be found in the literature, [4–6]; however, there are only few reports

A. Koeninger (✉) · G. Boehm · R. Meyer · M.-C. Amann
Lehrstuhl fuer Halbleitertechnologie E26, Walter Schottky
Institut, Technische Universitaet Muenchen, Am Coulombwall
4, 85748 Garching, Germany
e-mail: anna.koeninger@wsi.tum.de

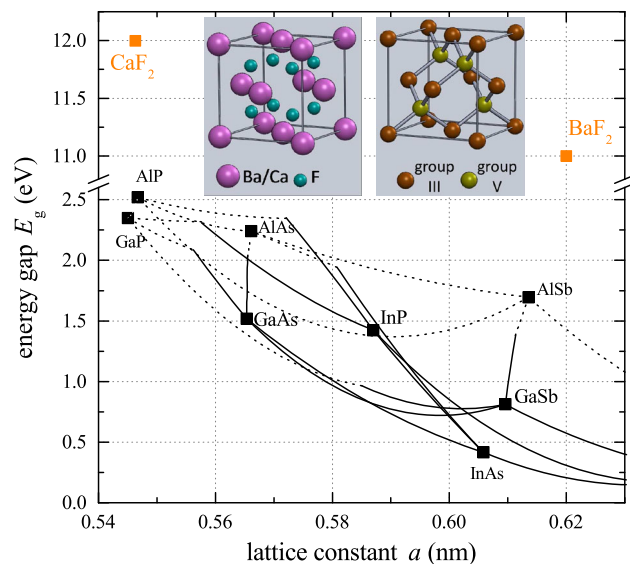


Fig. 1 Map of III–V semiconductors. A BaCaF₂ alloy can cover a multitude of III–V substrates. The *inserted pictures* show the fluorite lattice (*left*) and the zincblende lattice (*right*)—both are cubic lattices with a similar structure simplifying crystalline growth on top of one another

concerning the ternary material BaCaF₂, one example is Ref. [7]. Our aim in using the alloy was to achieve lattice matching. Thereby, the internal strain of the layers can be reduced in contrast to combinations of a binary group-IIa-fluoride with III–V semiconductors.

2 Experimental techniques

We used a Varian GEN II MBE system equipped with Ga, As₄, BaF₂ and CaF₂ effusion cells to grow on GaAs (100) substrates. About 3-mm-big crystallites of 99.99 % pure BaF₂ and CaF₂ served as fluoride source materials. As the fluorides sublime as undissociated molecular units, stoichiometry of the fluorides is given automatically [2, 7, 8]. After oxide removal in H₂SO₄, a preliminary GaAs surface treatment with fluorine was performed in an Oxford reactive ion etching (RIE) system. We found that this treatment was necessary to accomplish adhesion of subsequent BaCaF₂ layers. The aim was to create strong Ga–F bonds at the surface. X-ray photoelectron spectroscopy measurements only revealed a surface coverage of about 5 % of these bonds, but nonetheless we observed a significant improvement in layer stability. In the MBE system, we ramped up the substrate to a growth temperature of 500 °C and growth was performed at growth rates of 0.2 and 0.1 nm s^{−1} for GaAs and BaCaF₂, respectively. All temperatures mentioned represent thermocouple temperatures, with 500 °C_{TC} ≈ 500 °C_{pyro} and 720 °C_{TC} ≈ 620 °C_{pyro}.

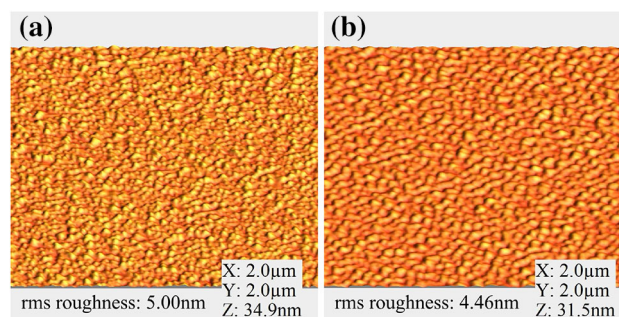


Fig. 2 AFM images of BaCaF₂ grown at different temperatures. Z is the maximum vertical height present in the scanned area of 2 × 2 μm². **a** T = 300 °C. **b** T = 500 °C

While our investigations are based on GaAs substrates, it should be possible to transfer these results to InP and GaSb substrates accordingly.

3 Results and discussion

3.1 Interface and surface

Previous to the DBR, we investigated the growth and structure of Ba_xCa_{1−x}F₂ grown on GaAs. Bearing in mind the great difference in thermal expansion coefficients between GaAs and the fluorides (at 300 K) from 5.83 × 10^{−6} K^{−1} for GaAs [9] to 19.9 × 10^{−6} K^{−1} and 19.3 × 10^{−6} K^{−1} for BaF₂ and CaF₂, respectively [10, 11], we worked with a BaF₂ content of x = 0.225, corresponding to lattice matching at 300 °C. This prevents the sample from cracking while it cools down from growth to room temperature as observed by other groups [5, 8]. The growth mode derived from atomic force microscope (AFM) images always was Volmer-Weber or island growth. Such images are depicted in Fig. 2: The sample shown in Fig. 2a was grown at 300 °C, the one shown in Fig. 2b at 500 °C. Both morphologies look similar. At 300 °C, the structures are slightly smaller and more random than at 500 °C. The root-mean-square (rms) roughness is in the same range, however. For the sample grown at 300 °C, it is 5.00 nm, and for the one grown at 500 °C, it is 4.46 nm. This is consistent with results from other groups that reported 3-D growth of the IIa-fluorides before [8, 12–14]. The samples always got a mirror-like surface with more or less grain boundaries, depending on growth temperature and rate.

The following sections will take a closer look at why grain boundaries occur and how they influence the properties of the material. Figure 3 shows the CaF₂–GaAs interface projected into two dimensions as Yamada et al.

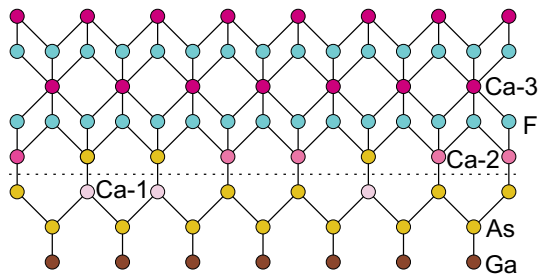


Fig. 3 Structural model of a CaF₂-GaAs interface: a transition layer contains different kinds of bonds leading to a nonabrupt interface [13]

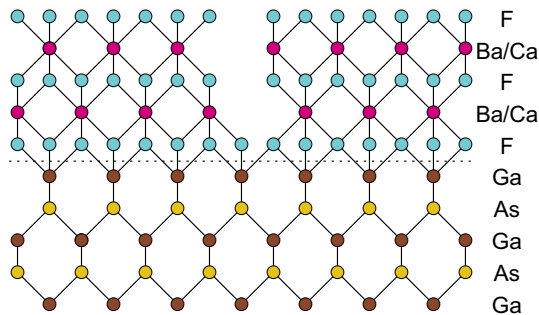


Fig. 4 Structural model of an ideal BaCaF₂-GaAs interface: There are two different possibilities for the lattice to start growing. The encounter then gives rise to a grain boundary

[13] proposed it in 1988. There is a transition layer present which contains different kinds of bonds between Ca and As or F. ‘Ca-1’ light pink circle stands for Ca-As bonds, ‘Ca-2’ medium dark pink circle for As-Ca-F bonds and ‘Ca-3’ dark pink circle stands for Ca-F bonds. Therefore, this is no abrupt interface. For adhesion reasons which are described more profoundly in Sect. 3.2, we tried to get a Ga-F interface as these are very strong bonds. Figure 4 shows an ideal model of this interface. The fluorite lattice contains twice the amount of fluorine atoms compared to arsenic atoms in the zincblende lattice. This leads to two different possibilities of how the BaCaF₂ lattice can start growing. On the left, the barium/calcium atoms occupy the lattice sites where gallium would have been in a zincblende lattice. On the right, they are shifted by one fluorine atom. So when two islands of these different orientations meet each other, a grain boundary is born.

We investigated the surface morphology of BaCaF₂ layers as a function of growth temperature and rate as shown in Fig. 5. In the process, the substrate temperature was not increased any further than 500 °C to prevent the formation of gallium droplets. The maximum growth rate was limited by the cell temperature of CaF₂ (1,200 °C). Different colors represent different shapes of areas surrounded by grain boundaries. Their average size in μm² is given by the inserted numbers. At 300 °C and growth rates

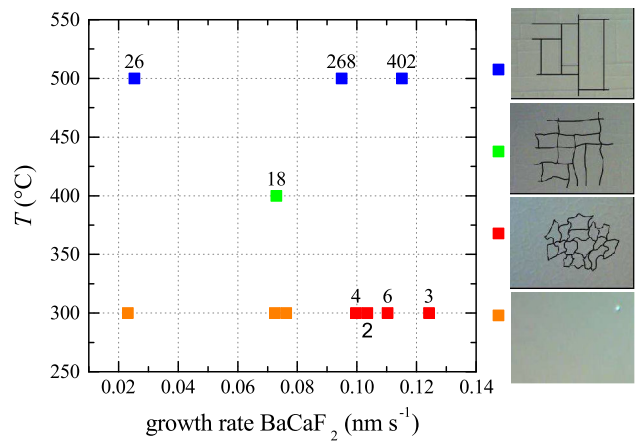


Fig. 5 Surface morphology plotted against growth temperature and rate for 270-nm-thick BaCaF₂ layers. Inserted numbers equal the average size of an area surrounded by grain boundaries in μm²

up to approx. 0.08 nm s⁻¹, no surface structures are visible with an optical microscope (filled orange square in Fig. 5). At higher growth rates, there are many grain boundaries, which are completely random (filled red square). More regular structures result from higher growth temperatures. While at 500 °C all grain boundaries are oriented parallel to the substrate’s [110] directions (filled blue square), at 400 °C, we find an intermediate form of oriented and random grain boundaries (filled green square). We explain these results by means of the surface mobility of incoming molecules during the growth process.

With increasing temperature, the surface mobility increases as well. So at low temperatures, we find many islands which result in many grain boundaries and thus in small areas surrounded by them. With higher temperatures, the molecules migrate further away on the surface and are able to adsorb at already existing islands. Thus, the structures get bigger and more regular meaning that there are less grain boundaries. Another reason why the area surrounded by grain boundaries increases with rising temperature is the occurrence of Ostwald ripening. For a surface, it is more favorable to have only few grain boundaries because this minimizes the interface energy. At high temperatures, there is a high diffusion rate, so that grain coarsening can occur as many small areas grow together to one big area. Thereby, surface energy is minimized [15, 16]. Furthermore, the kinetic energy of the molecules is increased at 500 °C compared to 300 °C. Therefore, growth oriented to the substrate is possible here.

The influence of the growth rate will be discussed next. Intuitively, one would assume that surface mobility is highest at high temperature and low growth rates. However, this is not found here reflected in the size of an area surrounded by grain boundaries, which increases from about 26 μm² at 0.025 nm s⁻¹ growth rate to 402 μm² at

0.115 nm s⁻¹ at 500 °C. An explanation is the Volmer-Weber growth mode of BaCaF₂, i.e., island growth. A low growth rate means little particle density on the surface. Thus, incoming molecules migrate on the surface but do not find others to adsorb to and consequently build a new island. According to Fig. 4, there are two possibilities for the molecules to start growing. Hence, the probability rises that two meeting islands are not oriented the same way leading to an increased number of grain boundaries. So at higher growth rates, these problems are reduced because incoming molecules can easier find existing adsorbates resulting in bigger islands of the same orientation and less grain boundaries. Considering this, the question arises whether the orange symbols in Fig. 5 ($T = 300$ °C, 0.02–0.08 nm s⁻¹ growth rate) really represent smooth surfaces. Or if they in fact consist of even smaller sized areas, which no longer can be resolved by our optical microscope. Also AFM measurements did not help here, as all images looked nearly the same.

A benefit of grain boundaries is that internal strain of the layers can be released there. Consequently, no classical pseudomorphic growth is possible. This is the reason why lattice matching could not be observed in X-ray diffraction (XRD) measurements and the corresponding BaF₂ content can only be estimated from predetermined growth rates of BaF₂ and CaF₂.

3.2 Long-term stability

If fluoride layers should be implemented in devices, it is necessary that they have a long lifetime. Fluorides have very strong bonds which cannot be broken easily, but they can be attacked by water. CaF₂ is nearly water-insoluble, whereas BaF₂ has a one hundred times higher water solubility of 0.16 g/(100 ml) at 25 °C [17]. Thus, the ternary material is supposed to be water-soluble, too. This is proven very well in Fig. 6 on the left, where the relationship between dissolving rate and BaF₂ content is displayed. In fact, we observed dissolving rates in de-ionized water of 0.28 to 3.17 nm min⁻¹ for BaCaF₂ layers of different crystalline quality. The dashed line represents a guide to the eyes, which shows that BaCaF₂ grown at 300 °C lies on the same curve as polycrystalline BaF₂ and CaF₂. On the right, the dissolving rates are displayed as a function of area surrounded by grain boundaries. For the BaCaF₂ sample represented by the orange triangle, we could not resolve the mean area surrounded by grain boundaries, and so we estimated it. With a numerical aperture of 0.95, the resolving power of the used microscope computes 0.289 μm. That is why a value of 0.0835 μm² was assumed for this sample. It is interesting to see that here the samples seem to lie on one curve, too. This indicates the grain boundaries representing the point of attack for water. As

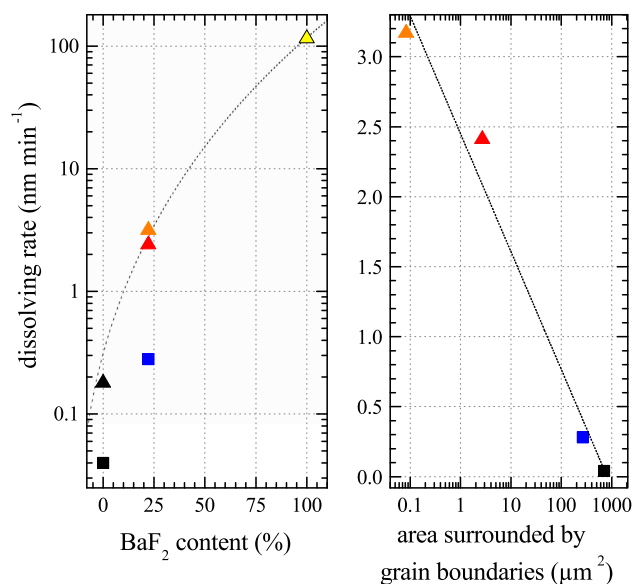


Fig. 6 Relationship between dissolving rate and barium content (*left*) and area surrounded by grain boundaries (*right*), respectively. *Triangle* represents polycrystalline material, *square* more crystalline material. *Black filled square* and *black filled triangle* stand for CaF₂, *yellow filled triangle* for BaF₂ and *orange filled triangle*, *red filled triangle* *blue filled square* for BaCaF₂, with the same properties as described in Fig. 5

already mentioned, BaCaF₂ layers grown at 300 °C showed much more grain boundaries than those grown at 500 °C, which beyond were closer oriented to the substrate. Consequently, these 300 °C-samples are dissolved faster as they offer a higher contact surface for water and thus behave similarly to polycrystalline materials. BaCaF₂ grown at 500 °C on the contrary acts more like a crystalline material. From this, we infer that a small number of grain boundaries represents a highly crystalline layer. This results in a resistant material leading to a high long-term stability in water. Of course, devices are usually not designed to work under water, but considering device lifetime, air humidity must not be neglected. The degeneration process in air will occur if the fluorides are not being protected by any kind of passivation layer.

As important as the prevention of creeping deterioration is the adhesion of the BaCaF₂ layers on GaAs. This was tested with a piece of adhesive tape being stuck on the surface and then being pulled off rapidly. Single layers with BaCaF₂ layer thicknesses of 270 nm showed good adhesion while layer stacks with only two pairs of GaAs/BaCaF₂ tend to peel off almost completely from the substrate. In order to improve adhesion at the very first interface, we made the GaAs surface more attractive to the fluoride molecules by providing F on the surface. Thus, bonding at the interface should be more stable. For this purpose, after de-oxidation in H₂SO₄, we exposed the substrate to a SF₆ plasma for 2 min. Subsequently, the

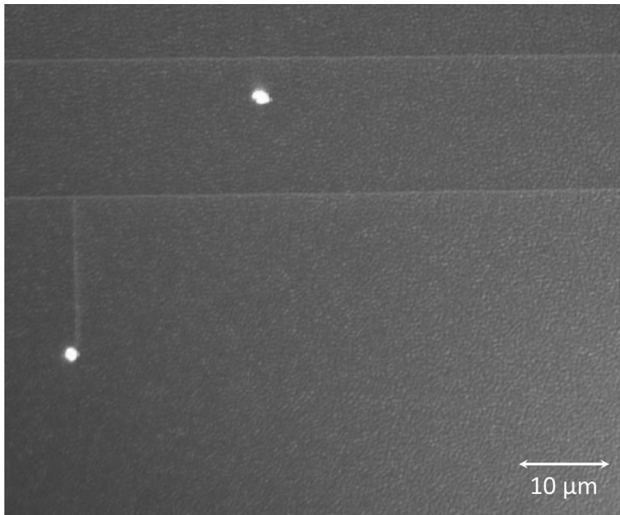


Fig. 7 Surface morphology of a three-pair GaAs/BaCaF₂-DBR grown by MBE observed with an optical microscope. The two bright spots are gallium droplets. Visible grain boundaries are parallel to the [110] directions of the (100) substrate

sample was immediately transferred into the MBE for BaCaF₂ growth. Indeed, samples prepared in this manner always passed the adhesion test.

So we can conclude that the growth of BaCaF₂ in a highly crystalline manner is successful on GaAs. According to our investigations, best results are achieved at a growth temperature of 500 °C and a growth rate of about 0.1 nm s⁻¹. However, a fluorination of the GaAs surface and in addition a passivation of the fluoride layers in order to secure long-term stability are highly recommended.

3.3 GaAs/BaCaF₂-DBR

The DBR was designed for a center wavelength of 1.55 μm, which results in quarter-wavelength layer thicknesses of 114 nm for GaAs and 270 nm for BaCaF₂, respectively. It was grown on a 2-inch GaAs (100) wafer at 500 °C. After every GaAs layer, we performed a fluorine functionalization step to ensure good adhesion of the subsequent fluoride layer. This three-pair Bragg mirror has a total thickness of only 1.2 μm. In comparison, an AlF₃/ZnS-DBR with the same reflectivity would be 2.5 μm thick. The surface morphology of our DBR is depicted in Fig. 7. As one can see, a few grain boundaries are present oriented parallel to the [110] directions of the GaAs substrate. Although surface roughness is kept within a limit (AFM rms roughness is 8.72 nm), it is not clear whether optical active layers can be grown on top. Further examination is necessary here.

We observed no peeling for this sample. So as a conclusion, the treatment with fluorine basically improved the stability of the layers.

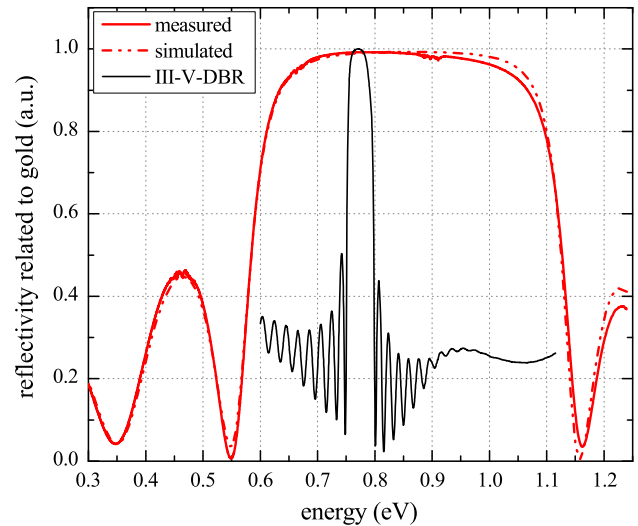


Fig. 8 Measured and simulated reflectivity (related to gold) of the GaAs/BaCaF₂ Bragg reflector. The high difference in refractive indices leads to a broad spectrum with a bandwidth (FWHM) of approx. 0.5 eV. In comparison, a DBR solely composed of III-V semiconductor materials achieves a bandwidth of only 0.05 eV

Figure 8 shows the reflectance spectrum of our GaAs/BaCaF₂ Bragg mirror as solid red line compared to a measurement of a state-of-the-art III-V-DBR (32 pairs of Al_{0.1}Ga_{0.37}In_{0.53}As/Al_{0.48}In_{0.52}As), solid black line. Obviously, the presented DBR's bandwidth (FWHM) is about a factor of ten larger than the one of a DBR being composed of III-V semiconductor materials only. This is due to the high contrast in refractive indices, $\Delta n \approx 2$, versus about $\Delta n \approx 0.3$ in III-V semiconductors. The dashed red line represents the reflectivity simulation of such a GaAs/BaCaF₂-DBR with a maximum reflectivity of 99.3 %, optical losses neglected. It is possible to fit the spectrum quite well. However, the layer thicknesses of the simulated DBR are detuned from the previously calculated values with 123 nm for the GaAs layers and 210 nm for the BaCaF₂ layers. This indicates that the growth rates were not correct and/or the refractive indices used in the calculations do not represent the true values applying to the grown materials. Bearing in mind the complex fabrication process of three separate epitaxies with fluorination in between, it is to be expected that the growth rates vary. However, the achieved reflectivity would be sufficient as top mirror in VCSEL or SESAM devices.

3.4 Thermal conductivity and resistivity

As heat generation and dissipation always are an issue for devices, thermal resistivity is an important parameter for each part of the device including the DBR. It was measured by evaluating the temperature-dependent electrical resistance of evaporated Pt stripes, following a method

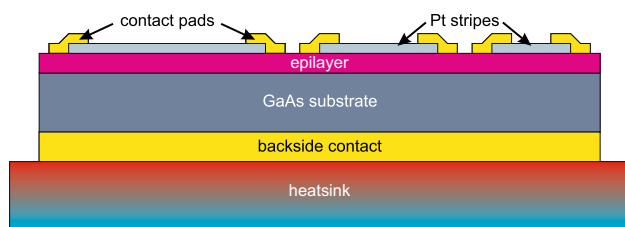


Fig. 9 Measuring principle for thermal resistivity measurements

described by Wada and Kamijoh [18]. In their approach, the thermal resistivity was determined by

$$R_{\text{th}} = \frac{\Delta T}{P}, \quad (1)$$

where ΔT is the temperature difference between Pt stripe and heatsink and P is the injected electrical power.

Figure 9 shows a schematic diagram of the measuring principle. To test this setup, we first determined the thermal conductivity of GaAs as this is a well-known value. Heat spreading in the substrate was considered according to (2)[19]

$$\lambda_{\text{th}} \approx \frac{\ln(4d/w)}{\pi R_{\text{th}} l}, \quad (2)$$

where λ_{th} is the thermal conductivity, d is the thickness of the layer or in this case of the substrate and w and l are width and length of the heat source, i.e., the Pt stripe. The measurements were done for values of w of 5, 10 & 15 μm and values of l of 500, 1,000 & 2,000 μm . The used substrates had a thickness of 350 μm . Thermal radiation was neglected in the calculations. Derived by this means, the measured values for GaAs range between 39.6 and 51.1 $\text{W K}^{-1} \text{m}^{-1}$. In average, this comes close to the literature value which is 46.0 $\text{W K}^{-1} \text{m}^{-1}$ [20]. Afterward, CaF_2 , BaCaF_2 and the DBR were measured the same way. Heat flow through the thin layer-stacks could be regarded as one-dimensional here.

For a heat-generating area (Pt stripe) of 30,000 μm^2 , the linear relationship of injected power and temperature difference for the examined samples is plotted in Fig. 10. According to (1), the slope of the $\Delta T(P)$ -curve equals the thermal resistivity of the layer stack. The data show that GaAs has the gentlest slope followed by CaF_2 and BaCaF_2 and the DBR having the steepest. This order is what is expected based on the literature values for the thermal conductivities. For one-dimensional heat flow, thermal conductivity and resistivity are linked via layer thickness and heat-generating area $A = w \times l$ [19],

$$\lambda_{\text{th}} = \frac{d}{R_{\text{th}} A}. \quad (3)$$

To obtain the actual values for CaF_2 , BaCaF_2 and the DBR, the thermal resistivity of the substrate has to be subtracted

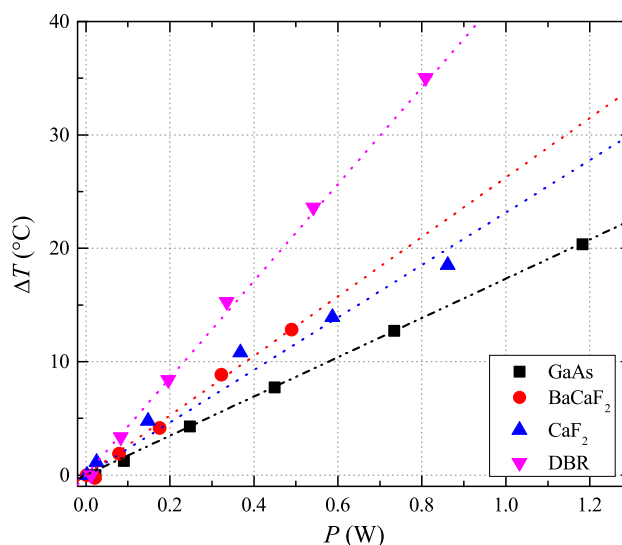


Fig. 10 Linear relationship of injected power and temperature difference for a GaAs substrate, CaF_2 and BaCaF_2 layers and the three-pair DBR. The slope is equivalent to the thermal resistivity of the measured layer stack in each case

first. However, the data points of CaF_2 do not fit the linear curve very well, and the thermal conductivity is much lower than it should be the case for crystalline CaF_2 . We retrieve a thermal conductivity of 1.97 $\text{W K}^{-1} \text{m}^{-1}$ in average but the literature value for CaF_2 is 9.7 $\text{W K}^{-1} \text{m}^{-1}$ [21]. This discrepancy can have different reasons. First, noncrystalline growth leads to a lower thermal conductivity. Second, weak bonding to the substrate increases the thermal resistivity, thus leading to a lower thermal conductivity, too. Finally, bad adhesion of the Pt stripes also influences the results negatively. For some stripes, peeling was observed.

Mixed crystals use to have a smaller thermal conductivity than their pure crystals due to alloy scattering [19]. Therefore, it is not surprising that the value for BaCaF_2 , 1.16 $\text{W K}^{-1} \text{m}^{-1}$, is smaller than that for CaF_2 . But just like the value for CaF_2 , we expected it to be higher.

The Bragg reflector has a thermal conductivity of 1.62 $\text{W K}^{-1} \text{m}^{-1}$. But for devices, thermal resistivity is the more comparable parameter. For a heat-generating area of 30,000 μm^2 , we determined a value of 24.5 K W^{-1} . In comparison, calculations for both AlGaInAs/AlInAs - and AlGaInAs/InP -Bragg mirrors with identical reflectivity reach values of 29.2 and 19.8 K W^{-1} , respectively. Thus, concerning thermal resistivity, our semiconductor/fluoride-DBR is in the same range with typical III–V alternatives although the total layer thickness, for example, compared to AlGaInAs/InP was only a fifth. However, the measured value was again larger than expected. We assume that in addition to the latter reasons, the GaAs– BaCaF_2 interfaces handicap heat conduction through the DBR. Possibly, the

thermal conductivity can be improved by increasing the amount of Ga–F bonds at the interfaces. Further improvements can be done here.

4 Conclusion

With implementation of the fluorine functionalization, we managed to grow a stable three-pair DBR of GaAs and BaCaF₂ on a full-wafer 2-inch GaAs (100) substrate. The optimal growth conditions for BaCaF₂ are at growth rates of about 0.1 nm s⁻¹ at 500 °C. With these parameters, the amount of grain boundaries is minimal resulting in the most crystalline fluoride material obtainable, which was also used in the DBR. The Bragg reflector had a broadband reflectance spectrum with a bandwidth of 0.5 eV at a total thickness of only 1.2 μm.

Due to the nonperfect surface morphology of BaCaF₂ layers, it is not recommended to use a III–V/fluoride-DBR below an optical active material. Thus, the variety of applicable VCSEL designs is limited. Apart from that, the thermal resistivity is not really improved compared to state-of-the-art semiconductor Bragg mirrors designed for the same reflectivity. However, the cavity length of a device using such a DBR is the smallest compared to III–V materials and even amorphous combinations. As surface morphology is not an issue for SESAMs, the material combination III–V/BaCaF₂ is probably more suitable for such applications.

In either case, by a further optimization of the Ga–F bonds at the III–V–BaCaF₂ interfaces, both durability and heat dissipation can be improved.

Acknowledgments The authors like to thank Prof. G. Franz (Munich University of Applied Sciences, Department 06) for helpful discussions concerning dry chemical etching.

References

1. S. Schön, M. Haiml, L. Gallmann, M. Achermann, U. Keller, in *2000 Proceedings Conference on Optoelectronic and Micro-electronic Materials and Devices (COMMAD)*, pp. 503–510 (2000)
2. E.H.C. Parker, *The Technology and Physics of Molecular Beam Epitaxy* (ISBN: 0306418606, Springer, 1985)
3. M.-C. Amann, M. Müller, in *12th International Conference on Transparent Optical Networks (ICTON)*, pp. 1–4 (2010)
4. S. Schön, M. Haiml, U. Keller, *Appl. Phys. Lett.* **77**(6), 782 (2000)
5. Z. Shi, H. Zogg, U. Keller, *J. Electron. Mater.* **27**(2), 55–58 (1998)
6. Z. Shi, H. Zogg, P. Müller, I.D. Jung, U. Keller, *Appl. Phys. Lett.* **69**, 3474–3476 (1996)
7. P.W. Sullivan, R.F.C. Farrow, G.R. Jones, *J. Cryst. Growth* **60**(2), 403–413 (1982)
8. H. Clemens, U. Stromberger, P.C. Weilguni, G. Bauer, *J. Appl. Phys.* **66**(4), 1680 (1989)
9. A.S. Jordan, *J. Cryst. Growth* **49**(4), 631–642 (1980)
10. P. Klocek, *Handbook of Infrared Optical Materials* (ISBN: 0824784685, Marcel Dekker Inc., New York, 1991)
11. S.S. Ballard, K.A. McCarthy, W.C. Davis, *Rev. Sci. Instrum.* **21**, 905–907 (1950)
12. M. Haiml, M. Achermann, U. Keller, *J. Vac. Sci. Technol. B* **18**(3), 1701–1705 (2000)
13. Y. Yamada, M. Oshima, S. Maeyama, T. Kawamura, T. Miyahara, *Appl. Surf. Sci.* **33–34**, 1073–1080 (1988)
14. T. Waho, F. Yanagawa, Y. Yamada, *J. Cryst. Growth* **95**(1–4), 415–420 (1989)
15. A. Baldan, *J. Mater. Sci.* **37**, 2171–2202 (2002)
16. P.W. Voorhees, *J. Stat. Phys.* **38**(1–2), 231–252 (1985)
17. D.R. Lide, *CRC Handbook of Chemistry and Physics*, 84th edn. (CRC Press Inc., Boca Raton, FL, 2003)
18. H. Wada, T. Kamijoh, *Jpn. J. Appl. Phys.* **35**, L648–L650 (1996)
19. L.A. Coldren, S.W. Corzine, *Diode lasers and photonic integrated circuits* (Wiley, New York, 1995)
20. S.M. Sze, *Semiconductor Devices: Physics and Technology*, 2nd edn. (ISBN: 0471333727, Wiley, New York, 2001)
21. B. Schumann, H. Neumann, *Cryst. Res. Technol.* **19**(1), K13–K14 (1984)